Check for updates

Received: 23 June 2023 | Revised: 28 October 2023 | Accepted: 10 November 2023

DOI: 10.1002/ese3.1624

ORIGINAL ARTICLE

Grid-tied PEMFC power conditioning system based on capacitor voltage thorough feedback procedure in a weak and harmonics-polluted network

Majid Hosseinpour[1] | **Tooraj Sabetfar**[1] | **Mahdi Shahparasti**[2]

[1]Department of Electrical Engineering, University of Mohaghegh Ardabili, Ardabil, Iran

[2]Department of Electrical Engineering and Energy Technology, School of Technology and Innovations, University of Vaasa, Vaasa, Finland

Correspondence
Majid Hosseinpour, Department of Electrical Engineering, University of Mohaghegh Ardabili, Ardabil, Iran.
Email: Hoseinpour.majid@uma.ac.ir

Abstract

Proton exchange membrane fuel cells (PEMFC) have been noticed by researchers due to their high efficiency, low pollution, and high-power density in distributed generation systems. In this paper, an LCL-type grid-tied PEMFC fuel cell power conditioning system is evaluated in a harmonics-polluted low-voltage grid. The LCL-filters can lead to resonance and instability despite their capability to attenuate harmonics. In this research, a transformer has been used to connect the fuel cell inverter to the grid. The grid-side inductor of LCL-filter is realized by the leakage inductance of the transformer. In addition, for more effective resonance damping and attenuation of current ripples caused by the grid voltage harmonics, a capacitor voltage comprehensive feedback control has been designed and investigated. The comprehensive feedback control of the capacitor voltage contains proportional, first and second-order derivative terms. In the proposed control scheme, the capacitor-current-feedback is opposed by the capacitor voltage derivative term due to reverse loop gain, which leads to deleting both of these loop gains. As a result, there is no need to utilize a current sensor in this control method. Consequently, the proportional and second-order derivative terms of the capacitor voltage attenuate the LCL-filter resonance. A low-pass filter is also considered in the second-order derivative loop in the controllable frequency range to ensure system stability. The simulation results of the PEMFC power conditioning system in different conditions confirm the proper attenuation of LCL resonance of grid-tied inverter, high-quality current injection to the harmonics polluted grid, the suitable stability, and the appropriate dynamic response for the proposed system. Under the proposed control scheme, the fuel cell power conditioning system demonstrates satisfactory stability. Even when reducing the LCL filter values by 5%–20%, the system maintains its stability effectively. Moreover, the THD of the injected current into the grid,

This is an open access article under the terms of the Creative Commons Attribution License, which permits use, distribution and reproduction in any medium, provided the original work is properly cited.
© 2023 The Authors. *Energy Science & Engineering* published by Society of Chemical Industry and John Wiley & Sons Ltd.

employing the proposed control strategy, has been successfully reduced to an impressive value of 1.97% in a weak and harmonical grid.

KEYWORDS
capacitor voltage thorough feedback control, current harmonics attenuation, LCL-type grid-tied PEMFC, system stability

1 | INTRODUCTION

Reducing fossil fuel reserves and increasing environmental pollution problems have caused researchers to consider renewable energy a cheap and clean energy source. Renewable energy includes wind, solar, geothermal, hydropower, fuel cell, and so on. A fuel cell is a suitable option for various applications due to its high reliability, low pollution, low maintenance requirement, and no use of moving devices.[1] Fuel cells are classified according to the type of electrodes, electrolytes, catalysts, and operating temperature. There are currently six types of fuel cells, including alkaline fuel cell (AFC), molten carbonate fuel cell (MCFC), phosphoric acid fuel cell (PAFC), proton exchange membrane fuel cell (PEMFC), solid oxide fuel cell (SOFC), and direct methanol fuel cell (DMFC).[2] PEMFC is widely utilized in distributed generation and hybrid systems due to its high-power density, solid electrolyte, low operating temperature, fast start-up, and suitable efficiency between 40% and 60%.[3] Solid oxide fuel cell (SOFC) is widely used in large-scale fuel cell power plants due to their high operating temperature, high efficiency, and high production energy compared to other fuel cells.[4] Higher energy efficiency than the internal combustion engine, as well as no pollution, has made the fuel cell one of the most modern sources of power generation in the transportation industry. Combining the fuel cell with secondary power supplies such as capacitors will provide advantages such as high-power density, fast start-up, and improved dynamic response.[5]

The fuel cell output voltage magnitude is low and inappropriate for grid-tied applications. Hence, using DC–DC converters, the fuel cell output voltage is boosted to an appropriate voltage level. In addition to improving the quality of the fuel cell output power, the DC–DC converter also helps to better control energy storage devices.[6,7] The produced AC voltage by the voltage source inverter (VSI) contains a significant harmonic distortion. So, to improve the quality of the output voltage, an interface filter is utilized between the inverter and the grid. Different network interface filters, including L, LC, LCL, and LLCL-filters are utilized.[8,9] Since in an L-type filter, only one inductor is responsible for reducing current harmonics, the inductor size or switching frequency must be high enough to improve the performance, as losses increase in both cases. The LC filter performs better at high frequencies and is smaller than the L filter. High inrush current and resonant frequency are the main disadvantages of LC filters.[10,11] The LCL-filter, which consists of a converter-side-inductor, a grid-side-inductor, and a capacitor, is smaller than the L filter. This type of filter has a better performance in eliminating harmonic content at high frequencies. Although, LCL-filters dampen the harmonics well, they can cause system resonance and instability. The use of resonance attenuation methods is necessary to ensure the stability of the LCL-based grid-tied systems.[12]

In general, resonance damping methods arising from LCL filters are divided into two categories: active damping methods[13,14] and passive damping methods.[15] Active damping methods are more favored due to their lower power losses, efficiency, and greater flexibility compared to passive damping methods. Among active damping methods, the following approaches are commonly employed: capacitor current feedback,[16] capacitor voltage feedback,[17] and LC-trap voltage or current feedback.[18] Active damping based on capacitor current feedback is one of the prevalent methods for damping LCL filter resonances.[19,20] By employing digital control and considering control delays, capacitor current feedback is treated as a virtual impedance that creates damping.[21] If the resonance frequency of the filter (f_r) is greater than one-sixth of the sampling frequency (f_s) ($f_r > f_s/6$), the virtual impedance behaves like a negative resistance, which leads to the creation of right-half-plane (RHP) poles and results in non-minimum phase behavior. To ensure system stability and prevent the generation of right-half-plane poles, the gain margin must be more precisely estimated. The requirements for gain margin can enhance the system's stability against network impedance changes but can also potentially lead to instability. To address the issue of gain margin requirements, a positive equivalent resistance can be used, which induces minimum phase behavior over a wide frequency range.[22] To extend the frequency range of the equivalent resistance, methods for reducing control

20505505, 2024, 1, Downloaded from https://ietjournals.onlinelibrary.wiley.com/doi/10.1002/cse2.1624 by University Of Yazd, Wiley Online Library on [04/03/2025]. See the Terms and Conditions (https://onlinelibrary.wiley.com/terms-and-conditions) on Wiley Online Library for rules of use; OA articles are governed by the applicable Creative Commons License

delays or compensating for control delays[23] can be employed.

Capacitor voltage through the feedforward procedure containing three terms of proportional, derivative, and second derivative of capacitor voltage can attenuate current distortion caused by grid voltage harmonics.[24,25] In a weak network, measuring grid voltage directly is challenging, and the voltage of common coupling point or PCC voltage is utilized instead. In several applications, the inverter is interconnected to the grid by adding a transformer,[26,27] and the grid-side-inductor of the LCL-filter is utilized by the transformer leakage inductance. In such a situation, the capacitor voltage of the LCL-filter is same as the PCC voltage. Unlike the grid-voltage-feedforward procedure, the capacitor-voltage-feedback scheme changes the current loop gain, which affects the stability of the system.[28] A capacitor-voltage-feedback procedure can remove LCL resonance completely, which is beneficial for system stability. In terms of digital control delay, the capacitor-voltage-feedback scheme can be considered as a virtual impedance (virtual resistor and virtual inductor) parallel to the filter capacitor. The virtual resistor dampens the LCL-filter resonance peak. Nevertheless, this equivalent virtual resistor may be negative and lead to right half-plane (RHP) poles in the open-loop transfer function of the system, which leads to a nonminimum phase behavior. If the virtual resistance is negative, the resonant frequency is between 1/3 and 1/2 of the sampling frequency, which causes system instability.[29] To ensure the stability of the system, the resonant frequency of the LCL-filter should be less than 1/3 of the sampling frequency. However, by correcting the digital control delay, the grid-tied inverter can maintain its stability in the presence of high-frequency harmonics.[23]

In this paper, capacitor-voltage-thorough-feedback (CVTF) scheme for an LCL-type grid-tied fuel cell power conditioning system is used to eliminate the grid current distortion caused by grid voltage harmonics. The CVTF scheme contains proportional, derivative, and second-order derivative terms of the LCL-filter's capacitor voltage. In the proposed control scheme, the capacitor-current-feedback (CCF) is opposed by the capacitor voltage derivative term due to the same symmetric loop gain. Thus, both of them can be deleted. As a result, the capacitor's current sensor is economized, and the resonance of the LCL-filter is attenuated by the proportional as well as second-order derivative terms of the capacitor voltage. To ensure that the equivalent resistance is positive at the Nyquist frequency that is the controllable frequency range, a low-pass filter is considered in the second-order derivative of the capacitor-voltage-feedback. Consequently, the grid-tied inverter can perform in a stable condition.

The structure of the rest of this paper is as follows: In Section 2, the materials and methods are presented. In this section, the structure of the investigated fuel cell is introduced, and the grid-tied fuel cell power conditioning system with LCL-filter is presented and analyzed. Then, in the continuation of the second part, the CVTF method is presented, and the shaping of the equivalent resistance using the CVTF scheme is presented. In Section 3, the simulation results are presented. In this section, the performance of the proposed system under the harmonic network voltage, as well as under reducing hydrogen fuel by 20% are simulated and analyzed. Finally, the last section concludes the article.

2 | MATERIALS AND METHODS

In this section, an overview of the proposed system for enhancing grid-connected fuel cell power quality will be provided. The proposed system involves a power generation unit based on a high-efficiency PEMFC, capable of producing around 10 kW of power, making it an attractive option for power generation at low-voltage levels. This power is first passed through a DC–DC converter and then injected into the grid using an inverter. To connect the inverter to the grid, an LCL filter is employed, along with a suitable control method to inject high-quality current into a weak and harmonic-rich grid. The step-by-step process of the proposed control system and parameter design will be elaborated further in the following subsections.

2.1 | Fuel cell

There are many methods and ideas for replacing fossil fuels. The utilization of fuel cells as a developing technology for producing clean energy has been proposed, recently. A fuel cell is an electrochemical converter that converts chemical energy into electrical energy, which uses no moving terms. Therefore, the simplicity of the structure, as well as the high efficiency, are the significant characteristics of the fuel cells. The fuel cell consists of two electric poles called electrodes, electrolyte, and catalyst. Hydrogen gas enters the anode electrode and is ionized by an oxidation reaction to a positive hydrogen ion (H^+) and a negatively charged electron (e^-). The fuel cell electrolyte only allows positive hydrogen ions to be transferred from the anode to the cathode and does not allow negative ions to be transferred. Electron transfer occurs through an external circuit and causes a direct DC. Figure 1 displays the general structure and function of the fuel cell.

20500505, 2024, 1, Downloaded from https://scijournals.onlinelibrary.wiley.com/doi/10.1002/cse3.1624 by University Of Yazd, Wiley Online Library on [04/03/2025]. See the Terms and Conditions (https://onlinelibrary.wiley.com/terms-and-conditions) on Wiley Online Library for rules of use; OA articles are governed by the applicable Creative Commons License

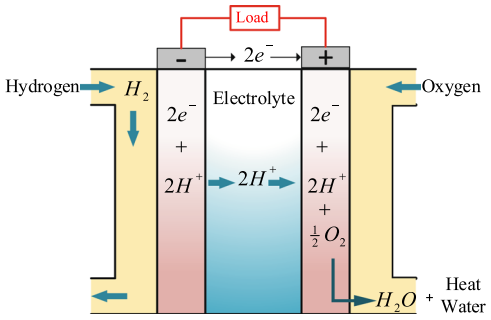

FIGURE 1 Proton exchange membrane fuel cell.

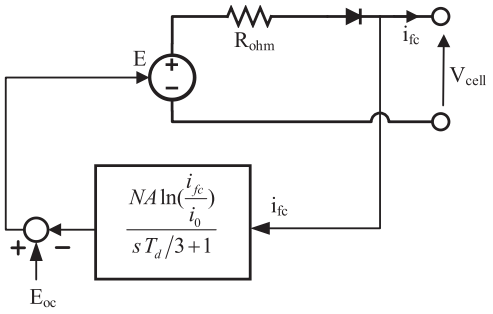

FIGURE 2 Fuel cell electrical model equivalent.

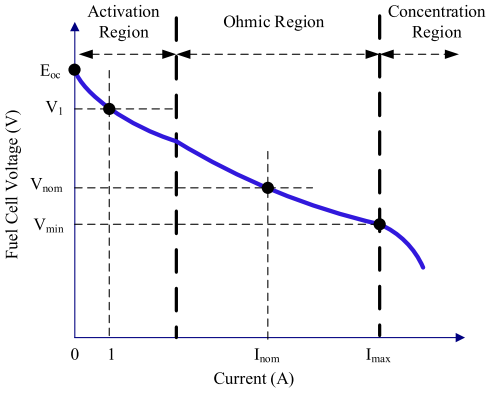

FIGURE 3 Fuel cell operating points regions.

The primary fuel for the fuel cell is hydrogen, but oxygen is also required to carry out the chemical reaction. Electrons enter the fuel cell from the cathode electrode, and during a reduction chemical reaction, electrons and protons combine with oxygen in the air to produce water. The chemical reactions that occur in a fuel cell at the anode and cathode are as follows:

1. The reaction on the anode side is as follows:

$$H_2 \rightarrow 2H^+ + 2e^-. \tag{1}$$

2. The reaction on the cathode side is as follows:

$$\frac{1}{2}O_2 + H_2 \rightarrow 2H^+ + 2e^- \rightarrow H_2O. \tag{2}$$

3. The total reaction is as follows:

$$\frac{1}{2}O_2 + H_2 \rightarrow 2H^+ + 2e^- \rightarrow H_2O + \text{heat} + \text{electricity}. \tag{3}$$

The operation of a PEMFC system is grounded in principles of thermodynamics, hydrodynamics, electrochemistry, and mass transfer theory. These components collectively form a complex nonlinear system, making it challenging to construct a comprehensive mathematical model. In this paper, an electrical model for PEMFC is employed to generate DC current and voltage. Equation (4) demonstrates the use of a nonlinear electrical model. The equivalent electrical model of a fuel cell is shown in Figure 2. From an electrical perspective, the fuel cell voltage–current (V–I) characteristic is described by the equation shown below:

$$V_{cell} = E_{oc} - NA\ln\left(\frac{i_{fc}}{i_0}\right).\frac{1}{sT_d/3+1} - R_{ohm}.i_{fc}. \tag{4}$$

Here, V_{cell} represents the fuel cell voltage, and the parameters E_{oc}, A, N, i_o, T_d, i_{fc}, and R_{ohm} correspond to the open-circuit voltage, Tafel slope, the number of cells, exchange current, the stack settling time, fuel cell current, and internal resistance, respectively.

As depicted in Figure 3, it is evident that the slope of the curve remains constant only within the ohmic region of the fuel cell V–I curve. In this region, as the voltage drops, the current rises. It is important to note that the V–I characteristic of the fuel cell introduces limitations on the device's performance. Following the activation stage, it is essential for the fuel cell voltage to fall within the range of V_{min} and V_1 to operate within the ohmic region. Consequently, the design of the power conditioning system must take these limitations into account to guarantee the stable performance of the system.

2.2 | Grid-tied fuel cell

The general structure of the grid-tied fuel cell power generation system is shown in Figure 4. The fuel cell generates DC voltage and a DC–DC converter is utilized to increase the output voltage, and an inverter is used to transfer the energy of the fuel cell to the AC network. As a result of the switching process, the VSI produce ripples that cause significant power quality problems in the

20500505, 2024, 1, Downloaded from https://ietresearch.onlinelibrary.wiley.com/doi/10.1002/cse3.1624 by University Of Yazd, Wiley Online Library on [04/03/2025]. See the Terms and Conditions (https://onlinelibrary.wiley.com/terms-and-conditions) on Wiley Online Library for rules of use; OA articles are governed by the applicable Creative Commons License

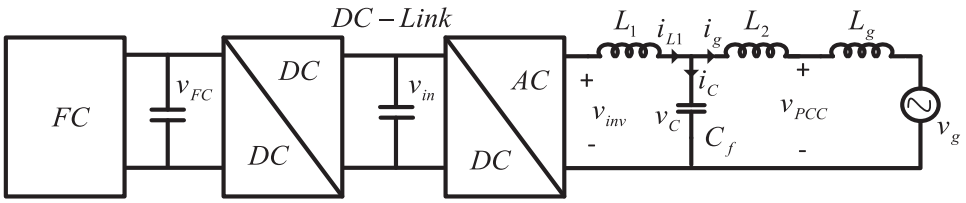

FIGURE 4 Grid-tied fuel cell structure with LCL-filter.

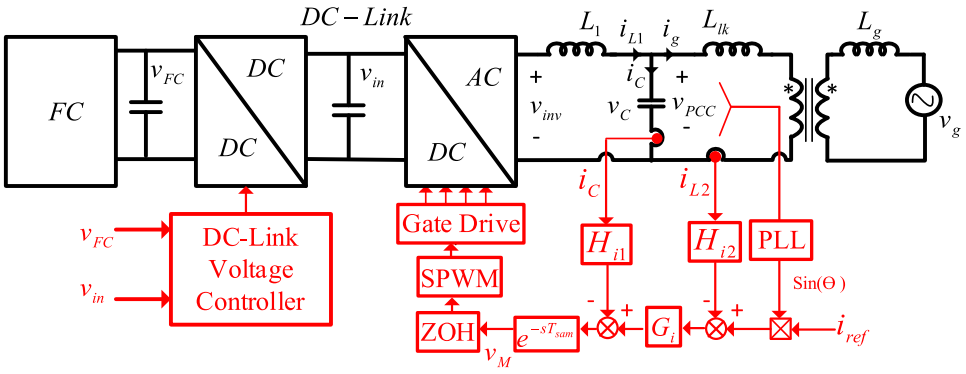

FIGURE 5 Overall power and control scheme for LCL-type grid-tied fuel cell inverter.

point of common coupling (PCC). When connecting fuel cells to the grid, an LCL-filter can be used to minimize the ripple generated by VSIs. The LCL-filter removes the voltage ripple but has zero impedance at the resonant frequency, which leads to unstable operation of the grid-tied inverter. For inverter stability, the resonance caused by the LCL-filter must be attenuated.

2.3 | The analysis of LCL-type grid-tied fuel cell inverter

Figure 5 displays the general structure of the grid-tied fuel cell power conditioning system with an LCL-filter and the general outline of the proposed control system. According to the figure, v_{inv}, v_{in}, and v_g are, respectively, the AC voltage generated by the inverter, the DC link voltage, and the grids voltage. The converter-side-inductor is represented by L_1, and the filter capacitor is considered as C_f. The inverter is interconnected to the network via a transformer with a turn ratio of $n_1/n_2 = 1$. Transformer leakage inductance is utilized as the LCL-filter grid-side-inductor. Therefore, in this control scheme, the filter capacitor voltage (v_C) is used as the PCC voltage (v_{PCC}). In general, grid impedance consists of an inductor and a resistor. The resistance on the grid side impedance prepares the attenuation consequence and contributes to the stability of the system. In the structure under study for grid impedance modeling, a pure inductor (L_g) is included to model the worst case in terms of control and stability. Hence, the equivalent grid-side-inductor (L_2) is as follows.

$$L_2 = L_{lK} + L_g.$$

To control the reference current (i_{ref}) with a control loop, the DC link voltage (v_{in}) can be compared with its reference value, and the amplitude of the current required for injection into the grid can be calculated. If the produced power of the fuel cell is increased, the DC link voltage will increase, and to stabilize it, the reference current must be increased. Thus, the balance of input and output power to the DC link capacitor determines the amplitude of the reference current injected into the grid.

The main purpose of the investigated control strategy of the grid-tied fuel cell power conditioning system is to control the injection current by the fuel cell to the grid so that it is in phase with the grid voltage and its harmonic content is minimized. Due to resonance in the LCL-filter, a single current loop is not sufficient to ensure the correct operation of the grid-tied inverter with the LCL-filter. In a conventional control scheme, CCF is usually utilized to dampen the LCL-filter resonance. Based on Figure 5, the mathematical control model of the grid-tied fuel cell power conditioning system with the LCL-filter is shown in Figure 6. $i_g(s)$ is the grid current that is sensed by the grid current sensor, and after comparison with the reference current $i_{ref}(s)$, its error is delivered to the current controller

20500505, 2024, 1, Downloaded from https://ietresearch.onlinelibrary.wiley.com/doi/10.1002/cse2.1624 by University Of Yazd, Wiley Online Library on [04/03/2025]. See the Terms and Conditions (https://onlinelibrary.wiley.com/terms-and-conditions) on Wiley Online Library for rules of use; OA articles are governed by the applicable Creative Commons License

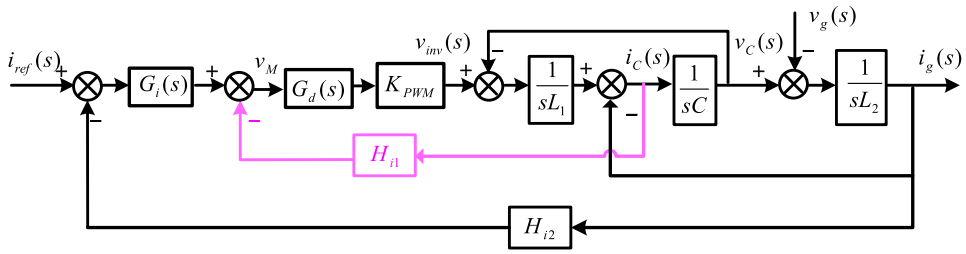

FIGURE 6 Control scheme of the LCL-type grid-tied fuel cell inverter under CCF strategy.

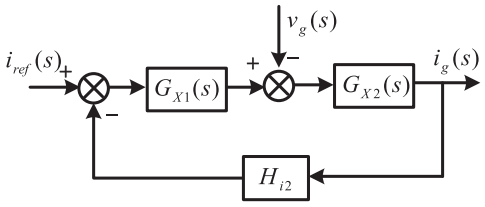

FIGURE 7 Equivalent control diagram of the grid-tied fuel cell inverter with LCL-filter.

$G_i(s)$. H_i is the gain of the capacitor-current sensor. The capacitor current $i_C(s)$ is subtracted from the current regulator output $G_i(s)$ to produce the modulation signal (v_M). The proportional-resonant (PR) compensator has a more significant gain at the fundamental frequency than the proportional-integral (PI) regulator and limits the steady-state error. Therefore, PR compensator, according to (5), has been utilized in this research.

$$G_i(s) = K_P + \frac{2K_r\omega_i s}{s^2 + 2\omega_i s + \omega_o}, \tag{5}$$

which ω_i is the bandwidth of the resonance term, and ω_o is the output angular frequency.

Conventional control methods for grid-tied inverters with LCL-filters can attenuate the harmonicas injected into the grid. However, the current harmonics caused by weak network distortion are difficult to eliminate. In the proposed method, a CVTF scheme is used to prevent current harmonics caused by grids' voltage distortions. The use of digital control causes a sampling delay, which is expressed by e^{-sTsam}, where T_{sam} represents the inverse of sampling frequency, that is half the switching cycle (T_{sw}) based on the Nyquist rate. The PWM delay due to zero-order hold (ZOH) is equivalent to half the sampling period.[30] The delay transfer function as $G_d(s) = e^{-1.5sTsam}$ with a period of 1.5 times the sampling period consists of the sum of the computational delay and the PWM delay. The $K_{PWM} = v_{in}/V_{tri}$ is the inverter bridge transfer function, or the inverter gain, in which V_{tri} is the maximum amplitude of the triangular carrier wave. In the system under study, unipolar Sinusoidal pulse width modulation (SPWM) switching pattern has been used for the grid-tied fuel cell inverter. Thus, the effective frequency of the harmonics appears to be twice the switching frequency ($2f_{s\omega}$).

2.3.1 | Grid current analysis

Using equivalent equations in Zheng et al.,[25] the functions of Figure 6 can be converted to the equivalent functions based on $G_{X1}(s)$ and $G_{X2}(s)$ according to Figure 7 using Mason's rule.

$$G_{x1}(s) = \frac{K_{pwm}G_d(s)}{s^2L_1C + sCH_{i1}K_{pwm}G_d(s) + 1}G_i(s), \tag{6}$$

$$G_{x2}(s) = \frac{s^2L_1C + sCH_{i1}K_{pwm}G_d(s) + 1}{s^3L_1L_2C + s^2L_2CH_{i1}K_{pwm}G_d(s) + s(L_1 + L_2)}. \tag{7}$$

According to Figure 7, $T_{ori}(s)$, the main loop current gain, and $i_{g\text{-}ori}(s)$, the main network current, can be expressed as follows:

$$T_{ori}(s) = G_{x1}(s)G_{x2}(s)H_{i2}, \tag{8}$$

$$i_{g,ori}(s) = \frac{1}{H_{i2}}\frac{T_{ori}(s)}{1 + T_{ori}(s)}i_{ref}(s) - \frac{G_{x2}(s)}{1 + T_{ori}(s)}v_g(s). \tag{9}$$

As can be seen in (9), the main current of the network $i_{g\text{-}ori}(s)$ consists of two parts, the first part is proportional to the reference current $i_{ref}(s)$, and the second part is proportional to the network voltage $v_g(s)$.

2.3.2 | Grid-voltage-full-feedforward (GVFF)

According to (9), to eliminate the grid current distortion caused by the grid voltage harmonics, a feedforward path from $v_g(s)$ is added to the $G_{x1}(s)$ output, as shown in

20500505, 2024, 1, Downloaded from https://ietresearch.onlinelibrary.wiley.com/doi/10.1002/cse2.1624 by University Of Yazd, Wiley Online Library on [04/03/2025]. See the Terms and Conditions (https://onlinelibrary.wiley.com/terms-and-conditions) on Wiley Online Library for rules of use; OA articles are governed by the applicable Creative Commons License

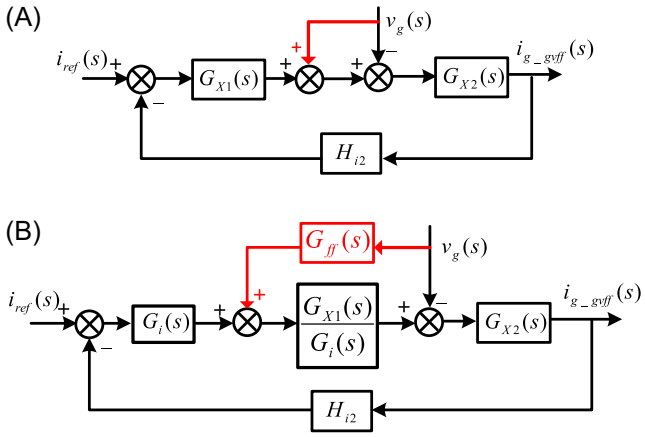

FIGURE 8 Grid-voltage-full-feedforward scheme, (A) Considering grid voltage feedforward, (B) Equivalent block diagram of Figure 8A.

Figure 8A. Therefore, an additional grid current relation based on the grid-voltage-feedforward is generated as follows:

$$i_{ga-gvff}(s) = \frac{G_{x2}(s)}{1 + T_{ori}(s)} v_g(s). \tag{10}$$

Then, by dividing $G_{x1}(s)$ by $G_i(s)$ and transferring the feedforward node of the grid voltage $v_g(s)$ to the output of the current regulator $G_i(s)$, the transfer function shown in Figure 8A is equivalent to the transfer function displayed in Figure 8B. The transfer function of the grid-voltage-feedforward $G_{ff}(s)$ is defined as follows:

$$G_{ff}(s) = \frac{G_i(s)}{G_{x1}(s)} = \frac{1}{K_{pwm}} \frac{1}{G_d(s)} + sCH_{i1} + \frac{s^2 L_1 C}{K_{pwm}} \frac{1}{G_d(s)}. \tag{11}$$

This feedforward procedure is named the GVFF scheme.

2.3.3 | CVTF

Direct measurement of the grid voltage $v_g(s)$ is a challenging issue. Because of the relationship between capacitor voltage and grid voltage, capacitor voltage measurement $v_C(s)$ is used instead of grids voltage $v_g(s)$ based on the following equation:

$$v_C(s) = v_g(s) + sL_2 i_g(s). \tag{12}$$

Using (12) and Figure 8B, Figure 9 demonstrates the equivalent grid-tied inverter's control block diagram

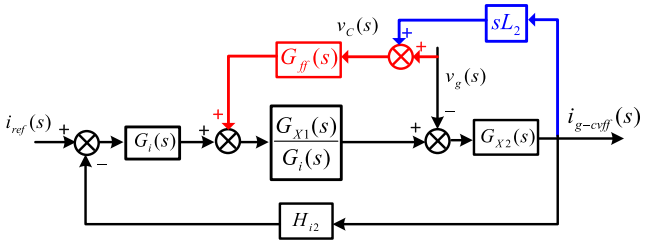

FIGURE 9 The grid-tied inverter's equivalent control diagram with CVTF scheme.

when the capacitor-voltage-feedback is used instead of the grid-voltage-feedforward. Based on (10), an additional term is obtained according to the following equation:

$$i_{ga-cvtf}(s) = \frac{G_{x2}(s)}{1 + T_{ori}(s)} [v_g(s) + sL_2 i_{g-cvtf}(s)]. \tag{13}$$

Therefore, the current injected into the grid in terms of capacitor voltage through the feedback scheme (CVTF) is as follows:

$$i_{g-cvtf}(s) = i_{g-ori}(s) + i_{ga-cvtf}(s). \tag{14}$$

Also, by replacing (9) and (13) in (14), the current injected into the grid based on CVTF by applying a component proportional to the reference current $i_{ref}(s)$ and a component proportional to the grid voltage disturbance $v_g(s)$ can be obtained as follows:

$$i_{g-cvtf}(s) = \frac{1}{H_{i2}} \frac{T_{ori}(s)}{1 + T_{ori}(s) - sL_2 G_{x2}(s)} i_{ref}(s) \tag{15}$$

As can be seen in (15), the component proportional to the grid voltage disturbance $v_g(s)$ is removed in the injected grid current. Therefore, disturbances caused by grids' voltage will not affect the injected grid current. The suggested method is named the CVTF scheme, which thoroughly represents the complete elimination of the current distortions caused by the grid voltage harmonics and distortions, that is equal to the feedforward procedure of the grid voltage. In (11), the expression $1/G_d(s)$ cannot be physically realized. Thus, the $G_d(s)$ is assumed to one,[31] and $G_{ff}(s)$ is expressed approximately as follows:

$$G'_{ff}(s) = \frac{1}{K_{pwm}} + sCH_{i1} + \frac{s^2 L_1 C}{K_{pwm}}. \tag{16}$$

20500505, 2024, 1, Downloaded from https://scijournals.onlinelibrary.wiley.com/doi/10.1002/cse3.1624 by University Of Yazd, Wiley Online Library on [04/03/2025]. See the Terms and Conditions (https://onlinelibrary.wiley.com/terms-and-conditions) on Wiley Online Library for rules of use; OA articles are governed by the applicable Creative Commons License

According to Figure 9 and by adding $G'_{ff}(s)$, the grid current is represented as follows:

$$i'_{ga-cvtf}(s) = G'_{ff}(s)\frac{G_{x1}(s)}{G_i(s)}\frac{G_{x2}(s)}{1+T_{ori}(s)}\Big[v_g(s)+sL_2 i'_{g-cvtf}(s)\Big], \tag{17}$$

$$\begin{aligned} i'_{g-cvtf}(s) &= i_{g-ori}(s) + i'_{ga-cvtf}(s) \\ &= \frac{1}{H_{i2}}\frac{T_{ori}(s)}{1+T_{ori}(s)-G'_{ff}(s)\frac{G_{x1}(s)}{G_i(s)}G_{x2}(s)sL_2} i_{ref}(s) \\ &\quad -\frac{\left(1-G'_{ff}(s)\frac{G_{x1}(s)}{G_i(s)}\right)G_{x2}}{1+T_{ori}(s)-G'_{ff}(s)\frac{G_{x1}(s)}{G_i(s)}G_{x2}(s)sL_2} v_g(s). \end{aligned} \tag{18}$$

By comparing (18) and (9), the current loop gain with the CVTF scheme (T'_{cvtf}) is expressed as follows:

$$T'_{cvtf} = \frac{T_{ori}(s)}{1-G'_{ff}(s)\frac{G_{x1}(s)}{G_i(s)}G_{x2}(s)sL_2}. \tag{19}$$

According to (6), (7), (8), (16), (19), T'_{cvtf} can be written as follows:

$$T'_{cvff} = \frac{G_i(s)G_d(s)K_{pwm}H_{i2}}{sL_1+(1+s^2L_1C)sL_2(1-G_d(s))}. \tag{20}$$

As seen in (16), the CVTF function includes the proportional term of $1/K_{PWM}$, the derivative term of s, CH_{i1}, and the second-order derivative term of s^2L_1C/K_{PWM}. According to Figure 6, the grid-tied inverter's control block diagram with the CVTF procedure is shown in Figure 10A. In this diagram, CCF is transmitted and replaced by capacitor-voltage-feedback. Thus, two loops counteract each other, one for the CCF and the other for the derivative term (sCH_{i1}). As a result, both loops can be removed, as shown in Figure 10B.

In the conventional CCF control scheme, a current sensor is used to measure the capacitor current. However, the capacitor voltage through the feedback scheme has a proportional term ($1/K_{PWM}$) and a second-order derivative term (s^2L_1C/K_{PWM}) of the capacitor voltage, and the active damping feedback of the capacitor current is removed. The resonance of the LCL-filter instead of the CCF term is attenuated by the second-order derivative and proportional terms of the capacitor voltage, which will be described in Section 4.

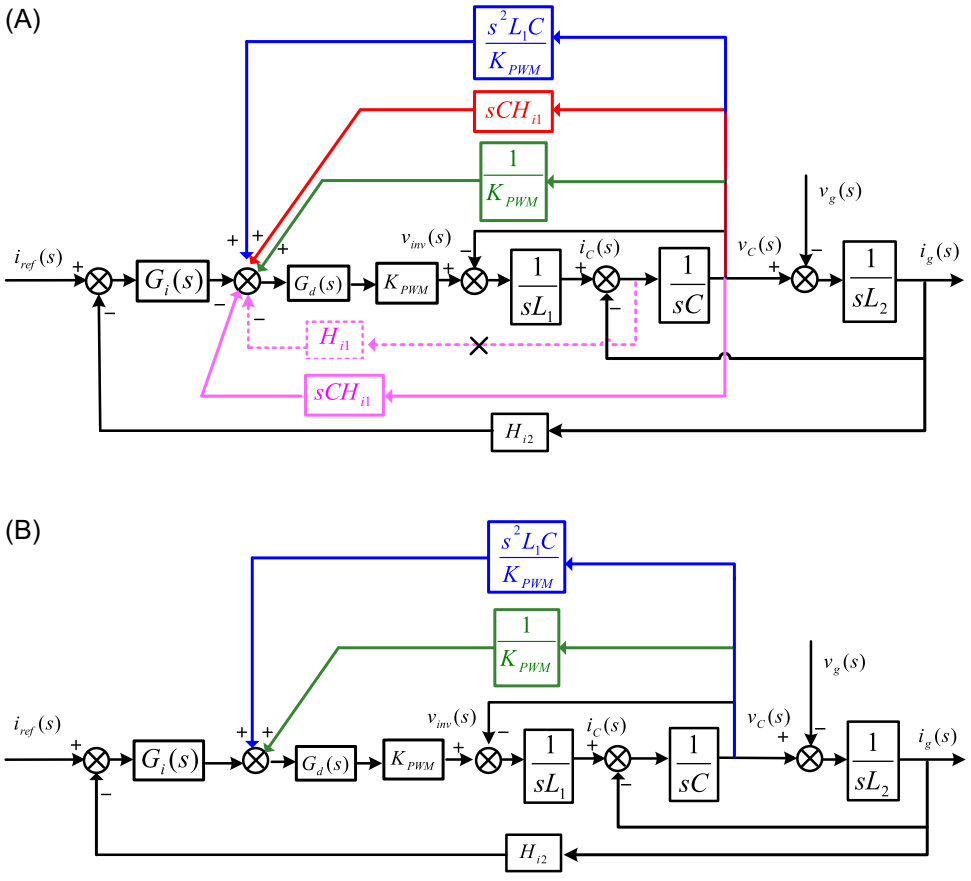

FIGURE 10 Fuel cell inverter control with CVTF scheme, (A) the main control scheme, and (B) simplified control scheme.

20500505, 2024, 1, Downloaded from https://ietresearch.onlinelibrary.wiley.com/doi/10.1002/cse3.1624 by University Of Yazd, Wiley Online Library on [04/03/2025]. See the Terms and Conditions (https://onlinelibrary.wiley.com/terms-and-conditions) on Wiley Online Library for rules of use; OA articles are governed by the applicable Creative Commons License

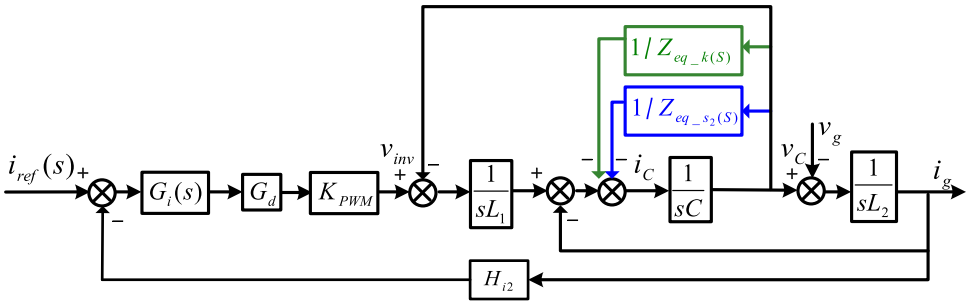

FIGURE 11 Block diagram of equivalent control of grid-tied fuel cell inverter with CVTF scheme.

2.4 | CVTF in stable systems

By moving the capacitor-voltage-feedback from the output of the current regulator to the input and modifying the function of the feedback path according to Figure 10B, a block diagram equivalent to Figure 11 is obtained.

The proportional term ($1/K_{PWM}$) and the second-order derivative of the capacitor-voltage-feedback can be considered equal by the virtual impedance $Z_{eq\text{-}k}$ and $Z_{eq\text{-}s2}$, respectively, that are connected in parallel to the filter capacitor. The phrases $Z_{eq\text{-}k}$ and $Z_{eq\text{-}s2}$ are expressed as follows:

$$Z_{eq-k}(s) = -\frac{sL_1}{G_d(s)}, \tag{21}$$

$$Z_{eq-s_2}(s) = -\frac{1}{sCG_d(s)}. \tag{22}$$

Substituting $s = j2\pi f$ in (21) and (22), these equations are obtained as follows.

$$\begin{aligned} Z_{eq-k}(j2\pi f) &= \frac{2\pi fL_1}{\sin(3\pi fT_{sam}) + j\cos(3\pi fT_{sam})} \\ &\triangleq R_{eq-k}(f) \| jX_{eq-k}(f) \end{aligned} \tag{23}$$

$$\begin{aligned} Z_{eq-s_2}(j2\pi f) &= -\frac{1}{2\pi fC\,[\sin(3\pi fT_{sam}) + j\cos(3\pi fT_{sam})]} \\ &\triangleq R_{eq-s_2}(f) \| jX_{eq-s_2}(f) \end{aligned} \tag{24}$$

where

$$R_{eq-k}(f) = \frac{2\pi fL_1}{\sin(3\pi fT_{sam})}, \tag{25}$$

$$X_{eq-k}(f) = \frac{2\pi fL_1}{\cos(3\pi fT_{sam})}, \tag{26}$$

$$R_{eq-s_2}(f) = -\frac{1}{2\pi fC\,\sin(3\pi fT_{sam})}, \tag{27}$$

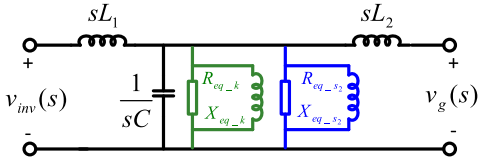

FIGURE 12 The virtual impedance equivalent by CVTF scheme.

$$X_{eq-s_2}(f) = \frac{1}{2\pi fC\,\cos(3\pi fT_{sam})}. \tag{28}$$

According to (23) and (24), and according to Figure 12, $Z_{eq\text{-}k}$ can be shown as a parallel connection of $R_{eq\text{-}k}$ resistance and $X_{eq\text{-}k}$ reactance. Similarly, $Z_{eq\text{-}s2}$ can be shown as a parallel connection of $R_{eq\text{-}s2}$ resistance with $X_{eq\text{-}s2}$ reactance.

$X_{eq\text{-}k}$ and $X_{eq\text{-}s2}$ cause the system resonance at the $\dot{f}_r$ frequency to deviate the LCL-filter resonance from the f_r frequency. If $R_{eq\text{-}k}$ and $R_{eq\text{-}s2}$ are positive, they participate in the resonance attenuation. If they are negative, they create some right-hand poles (RHP) in the open-loop transfer function, leading to system instability. According to (25) and (27), the $R_{eq\text{-}k}$ and $R_{eq\text{-}s2}$ curves can be depicted versus frequency. As shown in Figure 13, $R_{eq\text{-}s}$ is positive in the $(0, f_{sam}/3)$ range and negative in the $(f_{sam}/3, f_{sam}/2)$ range, while $R_{eq\text{-}s2}$ is negative in the $(0, f_{sam}/3)$ range and is positive in the $(f_{sam}/3, f_{sam}/2)$ range. Note that $f_{sam} = 1/T_{sam}$ is the sampling frequency.

The equivalent resistance (R_{eq}) can be expressed according to (29).

$$\begin{aligned} R_{eq}(f) &= R_{eq-k}(f) \| R_{eq-s_2}(f) \\ &= \frac{2\pi fL_1}{\sin(3\pi fT_{sam})[1 - (f/f_{r1})^2]}, \end{aligned} \tag{29}$$

where f_{r1} is the resonance frequency caused by L_1 and C, which is represented as follows:

20500505, 2024, 1, Downloaded from https://ietresearch.onlinelibrary.wiley.com/doi/10.1002/cse2.1624 by University Of Yazd, Wiley Online Library on [04/03/2025]. See the Terms and Conditions (https://onlinelibrary.wiley.com/terms-and-conditions) on Wiley Online Library for rules of use; OA articles are governed by the applicable Creative Commons License

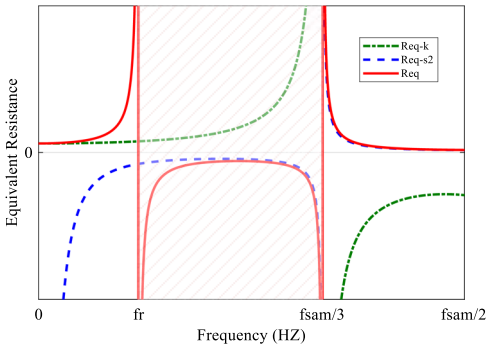

FIGURE 13 The curves of $R_{eq\text{-}k}$, $R_{eq\text{-}s2}$, and R_{eq} by frequency.

$$f_{r1} = \frac{1}{2\pi\sqrt{L_1 C}}. \tag{30}$$

Generally, the resonance frequency in stable systems is less than one-third of the sampling frequency ($f_{r1} < f_{sam}/3$). Thus, according to (29), the R_{eq} curve versus the frequency is shown in Figure 13. As can be seen, R_{eq} is positive in the (0, $f_{sam}/3$) and ($f_{sam}/3$, $f_{sam}/2$) range and negative in the (f_{r1}, $f_{sam}/3$) range. This means that the CVTF procedure may generate open-loop RHP, causing system instable condition, when the system resonance frequency is $\dot{f}_r \in (f_{r1}, f_{sam}/3)$. So, a positive R_{eq} in the fully controllable frequency range (0, $f_{sam}/2$) is expected to ensure system stability, which will be described in Section 5.

2.5 | Equivalent resistance shaping in CTVF scheme

2.5.1 | Equivalent resistance shaping by a low-pass filter

As shown in Figure 13, in the frequency (0, $f_{sam}/3$) range the resistance $R_{eq\text{-}k}$ is positive and $R_{eq\text{-}s2}$ is negative. To shape R_{eq} to a positive value, an easy approach is the increment of the $|R_{eq\text{-}s2}|$. Based on the equivalent block diagram and simplification from Figure 10B to Figure 11, the expression $1/Z_{eq\text{-}s2}$ corresponds to the second-order derivative term. Therefore, a weighting factor of less than one (K_w) can be considered in the second-order derivative term of capacitor voltage to increase the $|R_{eq\text{-}s2}|$ value. Therefore, $R_{eq\text{-}s2}$ is transformed as follows:

$$R'_{eq-s_2}(f) = -\frac{1}{K_w 2\pi f C \sin(3\pi f T_{sam})}. \tag{31}$$

According to (25) and (31), R_{eq} is shaped as follows:

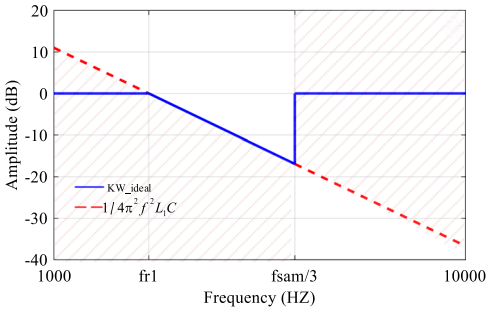

FIGURE 14 K_w range for positive R_{eq}.

$$R'_{eq}(f) = R'_{eq_k}(f)//R'_{eq_s_2}(f) = \frac{2\pi f L_1}{(1 - 4\pi^2 f^2 L_1 C K_W)\sin(3\pi f T_{sam})}. \tag{32}$$

The $sin(3\pi f T_{sam})$ phrase is positive for $f \in (0, f_{sam}/3)$ and is negative for $f \in (f_{sam}/3, f_{sam}/2)$. Hence R_{eq} to be positive, the $K_w < 1/(4\pi^2 f^2 L_1 C)$ expression requires to be true for the frequency range of $f \in (0, f_{sam}/3)$, and $K_w > 1/(4\pi^2 f^2 L_1 C)$ must be true for the frequency range $f \in (f_{sam}/3, f_{sam}/2)$. The range is shown in Figure 14 with the solid region.

Given the positive R_{eq}, the value of K_w to keep the harmonics elimination capability should be as close as possible to one. The ideal value for K_w is demonstrated in Figure 14 with a solid line. According to this figure, in the frequency range of (0, $f_{sam}/3$), the ideal K_w curve is same as the curve of amplitude-frequency for the second-order lowpass filter. If this lowpass filter is utilized to achieve K_w, the K_w requirements cannot be met in the ($f_{sam}/3$, $f_{sam}/2$) range. It should be noted that the second-order lowpass filter causes a phase delay. According to the equivalent block diagram and simplification from Figure 8B to Figure 9, the phase delay increases. $\angle Z_{eq\text{-}D2}$ indicates that the amplitude of the second-order lowpass filter in the frequency range of (f_{r1}, $f_{sam}/3$) should not be less than $1/(4\pi^2 f^2 L_1 C)$. Therefore, a first-order lowpass filter is utilized in this research.

2.5.2 | Design of a lowpass filter

Figure 15 displays a grid-tied inverter's block diagram with a CVTF scheme, in which a lowpass filter is included in the feedback path of the second-order derivative of the capacitor voltage.

Consequently, the capacitor-voltage-feedback function is represented as follows:

20500505, 2024, 1, Downloaded from https://ietresearch.onlinelibrary.wiley.com/doi/10.1002/cse2.1624 by University Of Yazd, Wiley Online Library on [04/03/2025]. See the Terms and Conditions (https://onlinelibrary.wiley.com/terms-and-conditions) on Wiley Online Library for rules of use; OA articles are governed by the applicable Creative Commons License

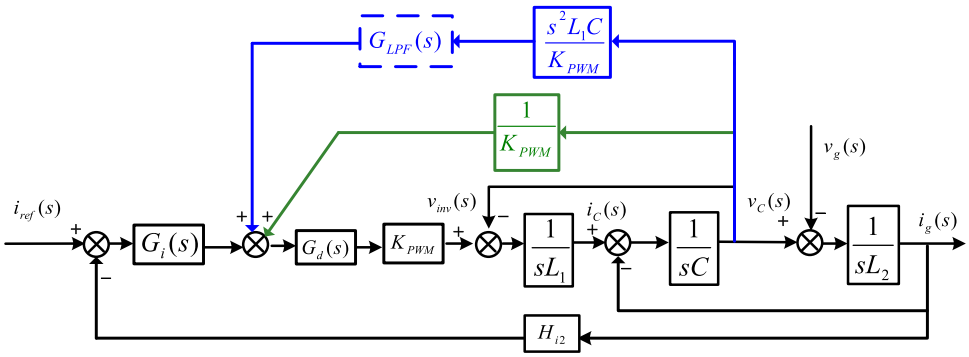

FIGURE 15 Simplified block diagram of grid-tied fuel cell inverter control with CVTF scheme by adding a low-pass filter.

$$G''_{ff}(s) = \frac{1}{K_{PWM}} + G_{LPF}(s)\frac{L_1 C}{K_{PWM}}s^2, \tag{33}$$

where $G_{LPF}(s)$ is a low-pass filter transfer function expressed as follows:

$$G_{LPF}(s) = \frac{1}{1 + s/(2\pi f_{c_LPF})}, \tag{34}$$

where f_{c_LPF} is the cutoff frequency. Using the low-pass filter, the $R_{eq\text{-}s2}$ phrase is changed as follows:

$$R'_{eq_s_2}(f) = -\frac{f^2_{c_LPF} + f^2}{2\pi f_{c_LPF} fC\left[f_{c_LPF}\sin(3\pi f T_{sam}) + f\cos(3\pi f T_{sam})\right]}. \tag{35}$$

According to (25) and (35), R_{eq} is shaped as follows:

$$R'_{eq}(f) = R_{eq_K}(f)//R'_{eq_s_2} - \frac{2\pi f L_1\left(f^2_{c_LPF} + f^2\right)}{af^2_{c_LPF} + bf_{c_LPF} + C}, \tag{36}$$

where

$$a = (1 - 4\pi^2 f^2 L_1 C)\sin(3\pi f T_{sam}), \tag{37}$$

$$b = -2\pi f^3 L_1 C\cos(3\pi f T_{sam}), \tag{38}$$

$$c = f^2\sin(3\pi f T_{sam}). \tag{39}$$

According to (36), the numerator of the phrase R'_{eq} is positive. Therefore, to create a positive R'_{eq}, it is necessary to:

$$af^2_{c_LPF} + bf_{c_LPF} + c > 0. \tag{40}$$

Since R_{eq} is positive in the $(0, f_{r1})$ frequency range without considering a positive low-pass filter, and the low-pass filter is effective in making a positive R_{eq}, equation (40) can only be true in the $f \in (f_{r1}, f_{sam}/2)$. In the $f \in (f_{r1}, f_{sam}/3)$, if $sin(3\pi f T_{sam}) > 0$ and $4\pi^2 f^2 L_1 C > 1$, then $a < 0$ will be resulted. As a result, according to (40), we will have the following:

$$f_1 < f_{c_LPF} < f_2, \tag{41}$$

where

$$f_1 = -\frac{b - \sqrt{b^2 - 4ac}}{2a}, \tag{42}$$

$$f_2 = -\frac{b + \sqrt{b^2 - 4ac}}{2a}. \tag{43}$$

In the frequency range of $f\in (f_{sam}/3, f_{sam}/2)$, if $sin(3\pi f T_{sam}) < 0$ and $4\pi^2 f^2 L_1 C > 1$, so $a > 0$ and $f_1 > f_2$. Therefore, according to (40), we will have the following:

$$f_{c_LPF} < f_2 \text{ or } f_{c_LPF} > f_1. \tag{44}$$

To shape R_{eq} positively in the $(0, f_{sam}/2)$ range, (40) must be true for each frequency in the range of $f\in(f_r, f_{sam}/2)$. Thus, f_{c_LPF} must be greater than the maximum value of f_1 in the $f\in(f_{sam}/3, f_{sam}/3)$ range and smaller than the minimum value of f_2 for $f \in (f_r, f_{sam}/3)$.

2.5.3 | Design sample

According to (41) and (42), with the described design procedure, a design example is given here. The parameters of the grid-tied fuel cell inverter are specified in Table 1. According to these parameters, the f_1 and f_2

20500505, 2024, 1, Downloaded from https://ietresearch.onlinelibrary.wiley.com/doi/10.1002/cse3.1624 by University Of Vaasa, Wiley Online Library on [04/03/2025]. See the Terms and Conditions (https://onlinelibrary.wiley.com/terms-and-conditions) on Wiley Online Library for rules of use; OA articles are governed by the applicable Creative Commons License

TABLE 1 The parameters of the investigated grid-tied fuel cell inverter.

Parameter	Value	Parameter	Value
Grid voltage (rms) (V_g)	220 V	Triangular wave Max amplitude (V_{tri})	4.578 V
Inverter side inductance (L_1)	460 μH	DC link voltage (v_{in})	360 V
Filter capacitance (C)	10 μF	Proportional coefficient (K_p)	0.0965
Trans. leakage inductance (L_{lk})	180 μH	Resonance Coefficient (K_r)	22
Grid frequency (f_o)	50 Hz	Inverter side current sensor gain (H_{i1})	0.013
Switching frequency (f_{sw})	10 kHz	Grid side current sensor gain (H_{i2})	0.15

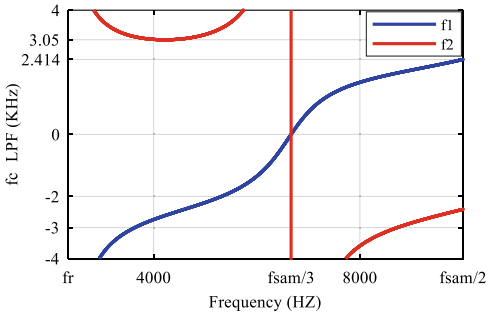

FIGURE 16 The curves of f_1 and f_2.

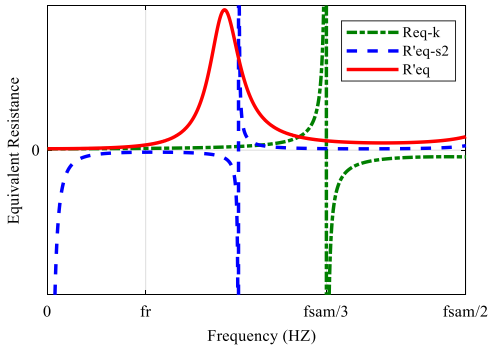

FIGURE 17 The curves of R_{eq_k}, R'_{eq_s2}, and R'_{eq} by frequency.

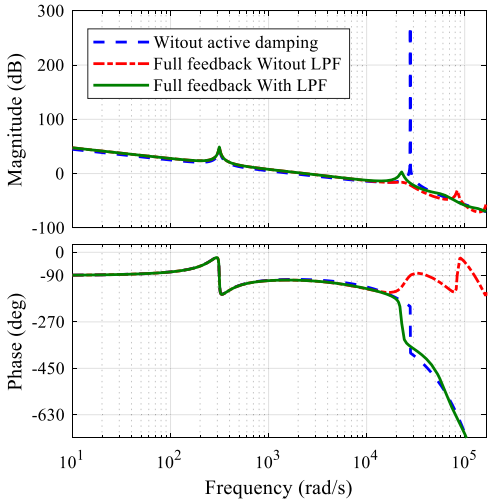

FIGURE 18 Bode plot of a grid-tied fuel cell inverter.

curves are shown in Figure 16. According to this figure, in the (f_{r1}, $f_{sam}/3$) range, the maximum f_1 value is zero, and the minimum value of f_2 is 3.55 kHz. While in the ($f_{sam}/3$, $f_{sam}/2$) range, the maximum value of f_1 is 2.414 kHz. Given that with a higher value of f_{c_LPF}, the harmonic attenuation capability is less affected, so $f_{c_LPF} = 3$ kHz is considered.

By substituting $f_{c_LPF} = 3$ kHz in (35) and (36), R'_{eq_s2} and R'_{eq} curves versus frequency can be plotted as shown in Figure 17. According to this figure, in the frequency range of (0, $f_{sam}/2$), R'_{eq} is positive, which is a satisfactory design requirement.

According to (5) and (16), the loop gain Bode plot of the grid-tied fuel cell inverter is shown in Figure 18. As can be seen, the resonance peak is damped when capacitor voltage through the feedback scheme is utilized. Nevertheless, there is a right-hand pole (RHP) pair, and the phase curve does not exceed −180°, so the stability of the system is not realized. By considering the low-pass filter to the second-order derivative term of capacitor voltage, there is no RHP in the open-loop transfer function. The cut-off frequency is $\omega_c = 3.1$ kHz, the phase margin is PM = 47.8°, and the gain margin is GM = 9.84 dB. Therefore, the system stability is ensured by the suggested capacitor-voltage-feedback scheme.

Figure 19 demonstrates the closed-loop zero and poles with different grid impedances (L_g). By changing the L_g from zero to 3 mH, all zeros and closed-loop poles of the system are within a unit circle. So, the suggested scheme of CVTF increases the stability and robustness of the system against changes in grid impedance.

2.5.4 | System sensitivity analysis

Sensitivity analysis provides information about system output based on changes in system component parameters under environmental conditions. In general, system sensitivity analysis is complex, and only the parts that play a significant role in the system stability are analyzed. In the analysis of LCL-filters, changes in the parameters of the inverter side and grid side inductances, as well as

20500505, 2024, 1, Downloaded from https://ietresearch.onlinelibrary.wiley.com/doi/10.1002/cse2.1624 by University Of Vaasa, Wiley Online Library on [04/03/2025]. See the Terms and Conditions (https://onlinelibrary.wiley.com/terms-and-conditions) on Wiley Online Library for rules of use; OA articles are governed by the applicable Creative Commons License

the filter capacitor, play a major role in the stability of the system. For the designed LCL-filter parameters, the THD value of the grid side current (i_g) is 1.97%, and the inverter side current (i_{L1}) is 9.1%. The probability of increasing the size of the inductor and capacitor is small. So, the sensitivity analysis has been investigated to reduce the LCL-filter parameters by 5% to 20% (Table 2).

To investigate the system stability and system requirements (GM > 3 dB and PM > 45°), Bode plots of the investigated system with changes in inductor and capacitor parameters of the LCL-filter are analyzed and shown in Figure 20. The initial value of the converter-side-inductor (L_1) is 460 mH and the grid-side-inductor (L_{lk}) is 180 mH. The first case is shown in Figure 20A for a 5% to 20% reduction in both filter inductors. Under these conditions, the phase margin and the gain margin, respectively are PM = 48.1° and GM = 10.9 dB, PM = 48.4° and GM = 11.6 dB, PM = 48.6° and GM = 11.9 dB, and finally, PM = 48.8° and GM = 12.1 dB, and the system has the appropriate stability. The second case is shown in Figure 20B for a 5% to 20% reduction in the capacitor and both filter inductors. Under these conditions, the phase margin and the amplitude margin, respectively are PM = 48.1° and GM = 12 dB, PM = 48.4° and GM = 13 dB, PM = 48.6° and GM = 13.5 dB, and finally, PM = 48.8° and GM = 13.8 dB, and the system has the suitable stability. The third case is shown in Figure 20C for a 5% to 20% reduction in the LCL-filter capacitor. In these conditions, the phase margin and the amplitude margin are PM = 47.8° and GM = 11.4 dB, PM = 47.8° and GM = 12.5 dB, PM = 47.8° and GM = 13.3 dB, and finally, PM = 47.7° and GM = 14.1 dB, respectively, and the system has the appropriate stability.

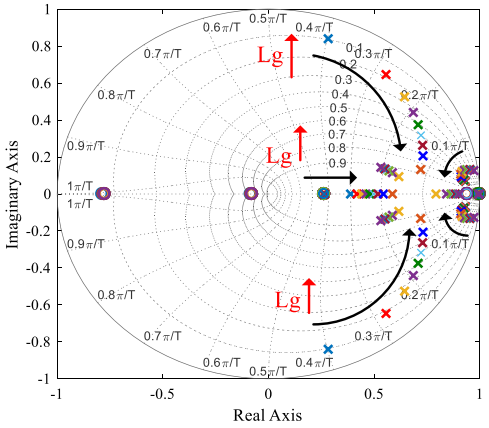

FIGURE 19 The zero-pole map for the grid-tied fuel cell inverter system under the CVTF scheme.

3 | RESULTS AND DISCUSSIONS

As mentioned in the first section, although the LCL filter has the capability to mitigate harmonics effectively, it can lead to resonance and system instability. To mitigate resonance and ensure system stability, this paper presents a full capacitor voltage

TABLE 2 Sensitivity analysis of the system under variation of filter parameters.

	Proposed control		Conventional control	
	THD of the inverter side current (i_{L1}) (%)	THD of the grid side current (i_g) (%)	THD of the inverter side current (i_{L1}) (%)	THD of the grid side current (i_g) (%)
5% reduction in L_1 & L_2	9.58	1.97	15.71	15.01
10% reduction in L_1 & L_2	1.11	1.98	16.08	15. 16
15% reduction in L_1 & L_2	10.74	1.99	16.49	15.32
20% reduction in L_1 & L_2	11.43	2.01	16. 93	15.45
5% reduction in C_f	9.12	1.97	15.44	14.84
10% reduction in C_f	9.14	1.97	15.51	14.84
15% reduction in C_f	9.14	1.99	15.59	14.84
20% reduction in C_f	9.18	2.02	15.66	14.84
5% reduction in L_1, L_2 & C_f	9.60	1.98	15.79	15.01
10% reduction in L_1, L_2 & C_f	10.17	1.99	16.23	15.16
15% reduction in L_1, L_2 & C_f	10.80	2	16.72	15.32
20% reduction in L_1, L_2 & C_f	11.52	2.03	17.25	15.47

20500505, 2024, 1, Downloaded from https://ietresearch.onlinelibrary.wiley.com/doi/10.1002/cse3.1624 by University Of Yazd, Wiley Online Library on [04/03/2025]. See the Terms and Conditions (https://onlinelibrary.wiley.com/terms-and-conditions) on Wiley Online Library for rules of use; OA articles are governed by the applicable Creative Commons License

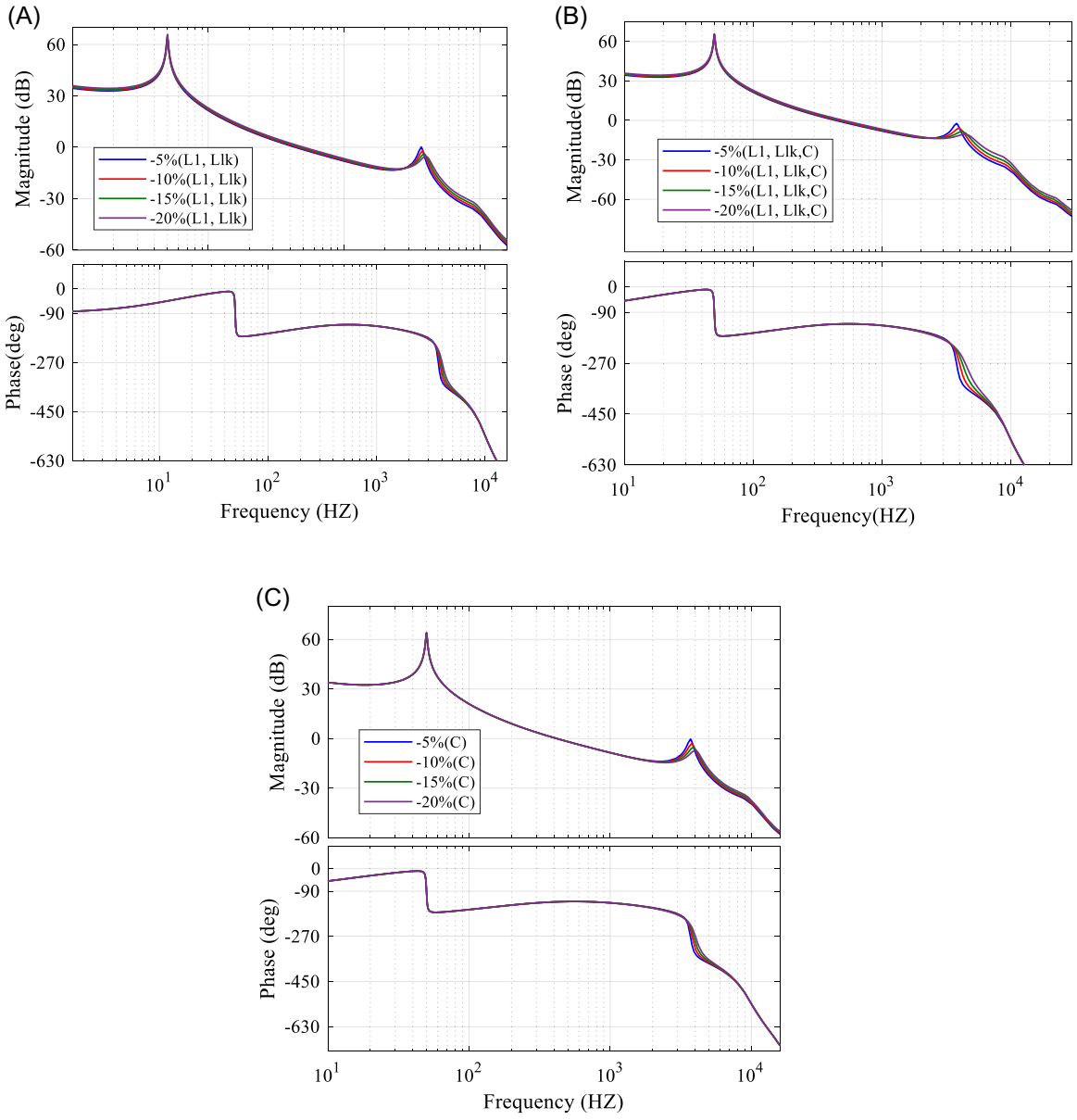

FIGURE 20 System stability analysis based on changes in LCL-filter parameters, (A) changes in the inverter side and grid-side-inductor, (B) changes in all parameters of the LCL-filter, (C) changes in the Capacitor.

feedback method, which, in contrast to the conventional and well-known capacitor current feedback method, possesses the capability to provide stability and inject high-quality current into a weak and harmonic-rich grid. After the control system is designed, the sensitivity and stability of the control system are evaluated for changes in the LCL filter parameters and for variations in the network impedance. Once the proper stability and low sensitivity of the control system are confirmed for a wide range of parameter variations, this section will present the simulation results of the grid-connected power conditioning fuel cell system. To achieve this, the performance of the system under investigation will first be assessed in a harmonic-rich grid, and then the system's power injection performance with a reduced hydrogen fuel supply will be evaluated.

The parameters of the grid-tied fuel cell inverter with an LCL-filter are presented in Table 1. Low voltage network impedance is usually modeled as an inductor and resistor. Since the resistor contributes to the stability of the grid-tied inverter, only an inductor is used as the grid impedance to investigate the worst case. The fuel cell employed in this study belongs to the PEMFC type. It provides a nominal voltage of 45 V, a power output of 6.5 kW, and operates at 65°C. The

20505052, 2024, 1, Downloaded from https://ietjournals.onlinelibrary.wiley.com/doi/10.1002/cse3.1624 by University Of Yazd, Wiley Online Library on [04/03/2025]. See the Terms and Conditions (https://onlinelibrary.wiley.com/terms-and-conditions) on Wiley Online Library for rules of use; OA articles are governed by the applicable Creative Commons License

power generation is achieved through the utilization of 65 individual cells.

3.1 | Performance of the proposed system under the harmonic network voltage

The results of grid-tied fuel cell inverter performance with grid impedance equal to $L_g = 2.6\,\text{mH}$ under the proposed control strategy in a weak and harmonic grid are shown in Figure 21. The THD values of the converter-side-inductor current (i_{L1}) and the grid-side-inductor current (i_g) with the proposed control strategy are 9.10% and 1.97%, respectively, which are shown in Figures 21A,B. Figure 21C displays the PCC voltage and the injected current to the network. Based on this figure, the PCC voltage and the injected grid current are in phase. Although the PCC voltage is highly distorted and contains significant low-order harmonics, the injected grid current does not contain any low-order harmonics, and its quality is very desirable. The quality of the injected grid current indicates the appropriate capability of the proposed control method. Figure 21D presents the power injected by the fuel cell power conditioning system into the grid. According to this figure, the proposed system injects 6.15 kW of power into the network.

The performance results of the studied fuel cell power generation system are shown in Figure 22. Figure 22A shows the fuel cell voltage, which is 43 V. This voltage is increased for connection to the grid by a DC-DC converter and reaches the required voltage of the network. In Figure 22B, the current of the fuel cell is shown to be 148 A. From the product of the voltage and current of the fuel cell, the output power of the fuel cell is obtained, which is approximately 6.4 kW and is shown in Figure 22C.

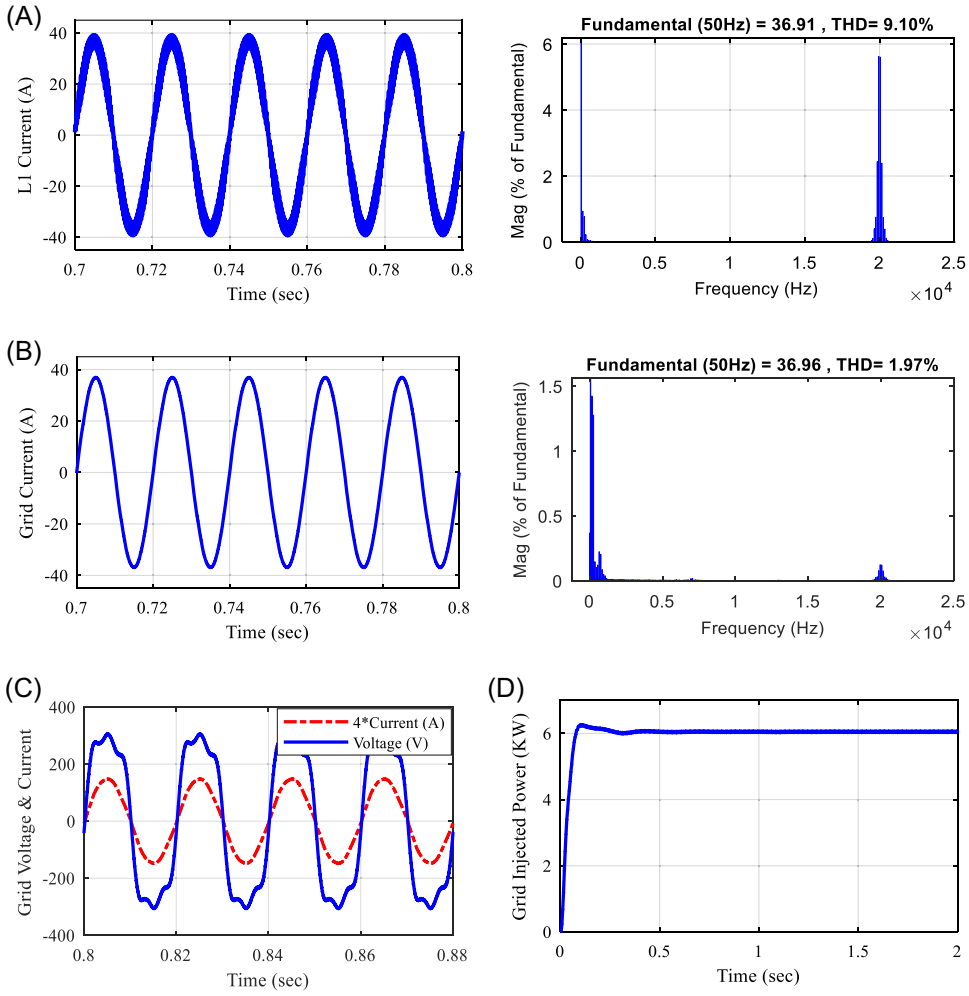

FIGURE 21 Operating result of the grid-tied fuel cell inverter under the proposed control strategy, (A) current and the converter-side-inductor THD, (B) network side inductor's current and THD, (C) PCC voltage and grid current, (D) power injected into the network.

20500505, 2024, 1, Downloaded from https://ietresearch.onlinelibrary.wiley.com/doi/10.1002/cse3.1624 by University Of Yazd, Wiley Online Library on [04/03/2025]. See the Terms and Conditions (https://onlinelibrary.wiley.com/terms-and-conditions) on Wiley Online Library for rules of use; OA articles are governed by the applicable Creative Commons License

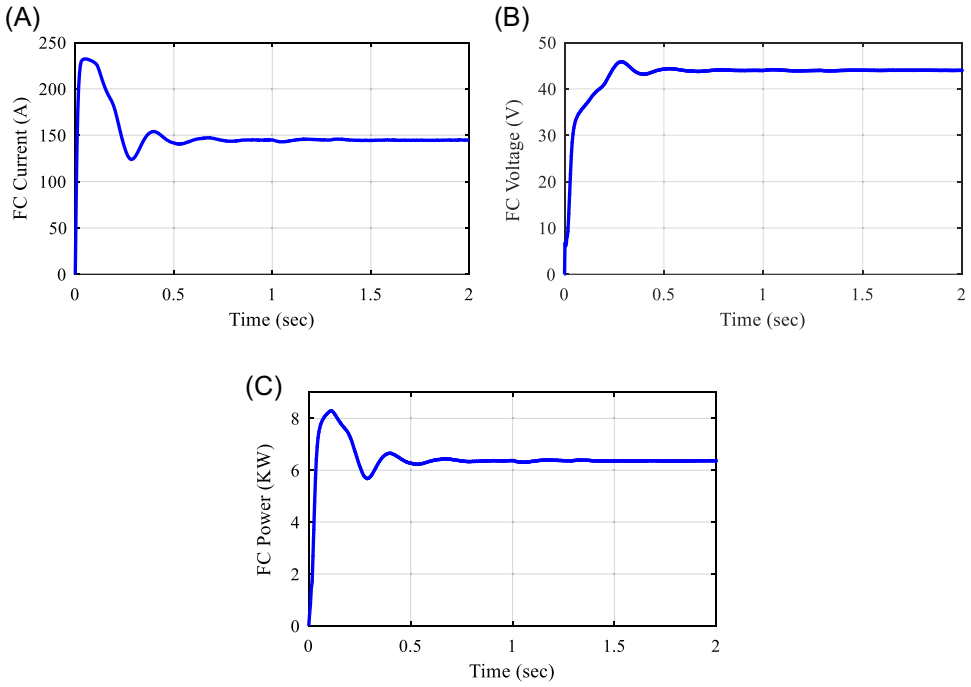

FIGURE 22 Fuel cell performance, (A) voltage, (B) current, and (C) produced power.

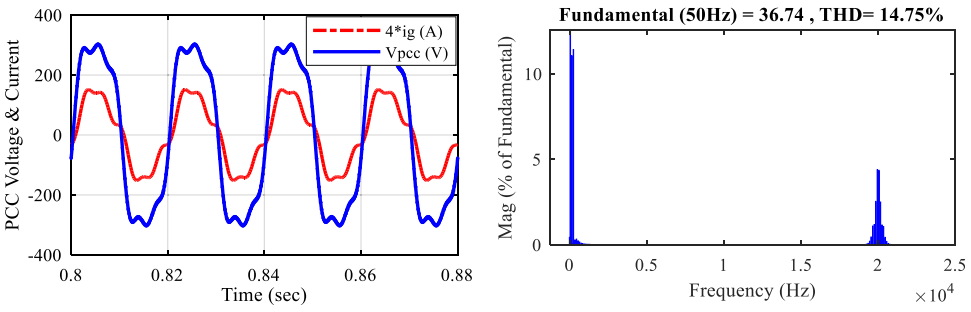

FIGURE 23 The function of grid-tied fuel cell inverter with conventional CCF scheme.

To compare the proposed control method with the conventional control method based on the CCF scheme, the performance of the conventional control method under the same conditions has been evaluated and compared. Figure 23 displays the PCC distorted and harmonical voltage and the grid injected current by the conventional control method. Since the CVTF is not used in the conventional CCF method and the inverter output impedance shaping is not evaluated, the quality of the injected current into the grid is not acceptable in a harmonics-polluted and weak network.

3.2 | Performance of the proposed system by reducing hydrogen fuel by 20%

Figure 24 presents the results of fuel cell performance to reduce fuel flow by 20%. According to the figure, in a period of 1–1.5 s, the fuel flow is reduced by 20%, and the production capacity of the fuel cell and the grid-injected current is also reduced. After this interval, the fuel flow and fuel cell production capacity returned to the normal condition. Figure 24A shows the grid-injected current that during the period of fuel flow reduction, the grid-injected current has decreased by about 20%. The voltage, current, and generated power of the fuel cell are shown in Figure 24B–D. As the fuel flow decreases, the fuel cell voltage decreases somewhat. But the main reduction occurs in the produced current of the fuel cell and decreases from 123 to 100 A. Eventually, the generated power of the fuel cell decreases in proportion to the amount of fuel flow reduction, from 6270 to 4850 W. Figure 24E presents the DC link voltage of the DC–DC converter output. The DC–DC converter increases the output voltage of

20500505, 2024, 1, Downloaded from https://ietresearch.onlinelibrary.wiley.com/doi/10.1002/cse2.1624 by University Of Vaasa, Wiley Online Library on [04/03/2025]. See the Terms and Conditions (https://onlinelibrary.wiley.com/terms-and-conditions) on Wiley Online Library for rules of use; OA articles are governed by the applicable Creative Commons License

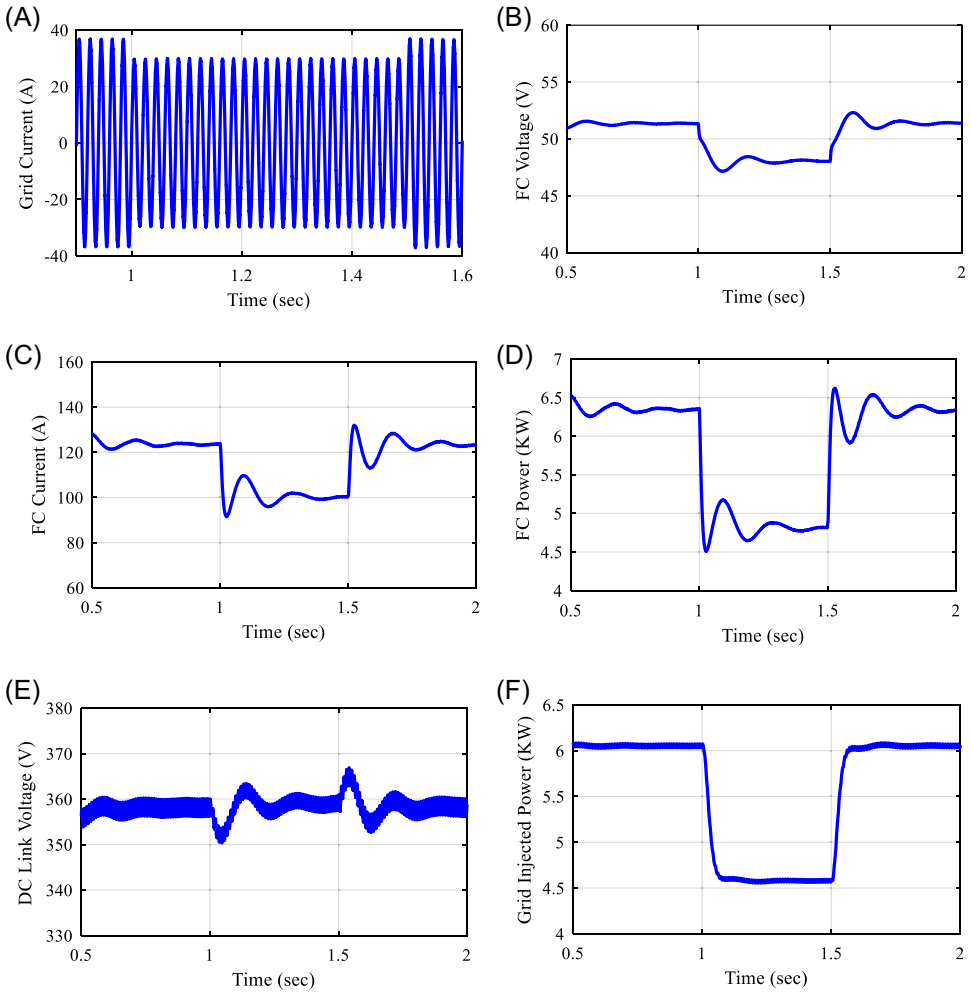

FIGURE 24 Grid-tied fuel cell inverter performance with 20% reduction in hydrogen fuel, (A) grid current, (B) fuel cell current, (C) fuel cell voltage, (D) fuel cell output power, (E) DC link voltage, and (F) power injected into the network.

the fuel cell to the desired value for connection to the grid by the inverter. Considering the effective voltage of the network equal to 220 V, the minimum value of DC link voltage should be $\sqrt{2}$ times of rms grid voltage. In this study, the reference value of DC link voltage is considered 360 V. The injected power to the grid is shown in Figure 24F. According to this figure, during the power flow reduction interval, the power injected into the network decreased by about 20% and decreased from 6030 to 4590 W. According to this figure, the appropriate operation of the DC link controller to determine the reference current (i_{ref}) to control the power injection into the network can be seen.

Finally, a comparison among the suggested control scheme with recent presented studies about grid-tied power conditioning systems in harmonics-polluted and weak grids is investigated in Table 3. According to this table, the current quality of the suggested scheme is more suitable.

TABLE 3 Comparison of the suggested scheme with various control schemes.

Applied method	Filter type	Controller	THD (%)
Presented in Lai et al.[32]	LC	Quasi-resonant	4.5
Presented in Guoqiao Shen et al.[33]	LCL	PR	2.2
Presented in Padmanaban et al.[34]	L	MPPT	2.8
Presented in Mohiuddin et al.[35]	LC	Partial feedback Linear controller	3.97
Presented in Li et al.[36]	LC	Active control + VPI	2.94
Presented in Patra et al.[37]	Hybrid filter	Backstepping control	1.89
Presented in Yang et al.[38]	LC	PR	2.88
Proposed	LCL	PR and CVTF	1.77

Abbreviation: CVTF, capacitor voltage thorough feedforward.

20505505, 2024, 1, Downloaded from https://ietresearch.onlinelibrary.wiley.com/doi/10.1002/cse3.1624 by University Of Yazd, Wiley Online Library on [04/03/2025]. See the Terms and Conditions (https://onlinelibrary.wiley.com/terms-and-conditions) on Wiley Online Library for rules of use; OA articles are governed by the applicable Creative Commons License

4 | CONCLUSION

In this paper, a CVTF control scheme is utilized to control an LCL-type grid-tied fuel cell power conditioning system. In addition to the resonant damping method, the proposed method also is capable of eliminating current distortion caused by the grid's voltage harmonics. The design based on CVTF consists of three parts, which include the proportional term ($1/K_{PWM}$), the proportional derivative, and the second-order derivative term of capacitor voltage. Given that the derivative term of the capacitor voltage is proportional to the CCF; Therefore, the effect is neutralized, and there is practically no need to use a capacitor current sensor in the proposed control method. To ensure the positive equivalent resistance to the Nyquist frequency, the low-pass filter (LPF) in the second-order derivative path is used. With the capacitor voltage through the feedback control method, the grid-tied fuel cell inverter operates stably in a harmonics-polluted and weak network and can attenuate the harmonics optimally. The grid-connected inverter of the fuel cell system under the proposed control strategy exhibits acceptable stability. Even with a 5%–20% reduction in the LCL filter inductor and capacitor values, the system's stability requirements, including a gain margin greater than 3 dB and a phase margin exceeding 45 degrees, are maintained. Additionally, the THD of the injected current into the grid using the proposed control strategy under the presence of harmonics in the weak network has reached the desirable value of 1.97%. The simulation results of the proposed grid-tied fuel cell power conditioning system show the ability of the proposed system to transfer the fuel cell power to the weak and harmonic-polluted network in stable and dynamic conditions.

ORCID

Majid Hosseinpour http://orcid.org/0000-0001-5074-4604
Tooraj Sabetfar http://orcid.org/0000-0002-3752-1497
Mahdi Shahparasti http://orcid.org/0000-0001-9994-0374

REFERENCES

1. Su Y, Ma K, Zheng S, Xue D, Li X. Rigdelet neural networks-based maximum power point tracking for a PEMFC connected to the network with interleaved boost converter optimized by improved satin bowerbird optimization. *Energy Reports*. 2023;9:4960-4970.
2. Fan L, Tu Z, Chan SH. Recent development of hydrogen and fuel cell technologies: a review. *Energy Reports*. 2021;7:8421-8446.
3. Kim BM, Choi YH, Yoo SJ. Adaptive control of proton exchange membrane fuel cell air supply systems with asymmetric oxygen excess ratio constraints. *IEEE Access*. 2020;8:5537-5549.
4. Yuan X, Liu Y, Bucknall R. A novel design of a solid oxide fuel cell-based combined cooling, heat and power residential system in the UK. *IEEE Trans Ind Appl*. 2021;57:805-813.
5. Xun Q, Liu Y, Huang X, Grunditz EA, Zhao J, Zhao N. Drive cycle energy efficiency of fuel cell/supercapacitor passive hybrid vehicle system. *IEEE Trans Ind Appl*. 2021;57(1):894-903.
6. Dastgiri A, Hosseinpour M, Sedaghati F, Mousavi-Aghdam SR. A high step-up DC–DC converter with active switched LC-network and voltage-lift circuit: topology, operating principle, and implementation. *Int J Circuit Theory Appl*. 2022;50(1):226-248.
7. Hosseinpour M, Ahmadi M, Seifi A, Mousavi-Aghdam SR. A new transformerless semi-quadratic buck–boost converter based on combination of Cuk and traditional buck–boost converters. *Int J Circuit Theory Appl*. 2022;50(11):3926-3948.
8. Rasekh N, Hosseinpour M. LCL filter design and robust converter side current feedback control for grid-connected proton exchange membrane fuel cell system. *Int J Hydrogen Energy*. 2020;45(23):13055-13067.
9. Rasekh N, Rahimian MM, Hosseinpour M, Dejamkhooy A, Akbarimajd A. A step by step design procedure of PR controller and capacitor current feedback active damping for a LCL-type grid-tied T-type inverter. *2019 10th International Power Electronics, Drive Systems and Technologies Conference (PEDSTC)*. IEEE. 2019:612-617.
10. Ma K, Tang W, Cheng R, Song Y. Modeling of interconnected voltage and current controlled converters with coupled LC–LCL filters. *IEEE Trans Power Electron*. 2021;36(4):3995-4005.
11. Hosseinpour M, Rasekh N. A single-phase grid-tied PV based trans-z-source inverter utilizing LCL filter and grid side current active damping. *J Energy Manage Technol*. 2019;3(3):67-77.
12. Chowdhury VR, Kimball JW. Robust control scheme for a three phase grid-tinverter with LCL filter during sensor failures. *IEEE Trans Ind Electron*. 2021;68(9):8253-8264.
13. Hosseinpour M, Dastgiri A, Shahparasti M. Design and analysis of a power quality improvement system for photovoltaic generation based on LCL-type grid connected inverter. *Int J Eng*. 2023;37(2):252-267.
14. Hosseinpour M, Asad M, Rasekh N. A step-by-step design procedure of a robust control design for grid-connected inverter by LCL filter in a weak and harmonically distorted grid. *Iran J Sci Technol Trans Electr Eng*. 2021;45:843-859.
15. Kouchaki A, Nymand M. Analytical design of passive LCL filter for three-phase two-level power factor correction rectifiers. *IEEE Trans Power Electron*. 2018;33(4):3012-3022.
16. Rasekh N, Hosseinpour M. Adequate tuning of LCL filter for robust performance of converter side current feedback control of grid connected modified–y-source inverter. *Int J Industr Electron Control Optim*. 2020;3(3):365-378.
17. Xin Z, Loh PC, Wang X, Blaabjerg F, Tang Y. Highly accurate derivatives for *LCL*-filtered grid converter with capacitor voltage active damping. *IEEE Trans Power Electron*. 2016;31(5):3612-3625.

20500505, 2024, 1, Downloaded from https://ietresearch.onlinelibrary.wiley.com/doi/10.1002/cse3.1624 by University Of Yazd, Wiley Online Library on [04/03/2025]. See the Terms and Conditions (https://onlinelibrary.wiley.com/terms-and-conditions) on Wiley Online Library for rules of use; OA articles are governed by the applicable Creative Commons License

18. Huang M, Wang X, Loh PC, Blaabjerg F. Active damping of *LLCL*-filter resonance based on *LC*-trap voltage or current feedback. *IEEE Trans Power Electron*. 2016;31(3):2337-2346.
19. Hosseinpour M, Kholousi A, Poulad A. A robust controller design procedure for LCL-type grid-tied proton exchange membrane fuel cell system in harmonics-polluted network. *Energy Sci Eng*. 2022;10(10):3798-3818.
20. Rasekh N, Hosseinpour M, Dejamkhooy A, Akbarimajd A. Robust power conditioning system based on LCL-type quasi-y-source inverter for grid connection of photovoltaic arrays. *Int J Autom Control*. 2021;15(6):692-709.
21. Pan D, Ruan X, Bao C, Li W, Wang X. Capacitor-current-feedback active damping with reduced computation delay for improving robustness of LCL-type grid-connected inverter. *IEEE Trans Power Electron*. 2014;29(7):3414-3427.
22. He Y, Wang X, Ruan X, Pan D, Xu X, Liu F. Capacitor-current proportional-integral positive feedback active damping for LCL-type grid-connected inverter to achieve high robustness against grid impedance variation. *IEEE Trans Power Electron*. 2019;34(12):12423-12436.
23. Li X, Fang J, Tang Y, Wu X, Geng Y. Capacitor voltage feedforward with full delay compensation to improve weak grids adaptability of LCL-filtered grid-connected converters for distributed generation systems. *IEEE Trans Power Electron*. 2018;33(1):749-764.
24. Wang X, Qin K, Ruan X, Pan D, He Y, Liu F. A robust grid-voltage feedforward scheme to improve adaptability of grid-connected inverter to weak grid condition. *IEEE Trans Power Electron*. 2021;36(2):2384-2395.
25. Zheng Z, Zhang L, Wang Y, Lei Z, Zou Y, Wu C. Full grid voltage feedforward for critical mode LCL-type single-phase grid-tied inverters with physical interpretations. *IEEE Trans Power Electron*. 2023;38(4):5283-5295.
26. Liu Q, Li Y, Hu S, Luo L. A transformer integrated filtering system for power quality improvement of industrial DC supply system. *IEEE Trans Ind Electron*. 2020;67(5):3329-3339.
27. Liu Q, Li Y, Luo L, Peng Y, Cao Y. Power quality management of PV power plant with transformer integrated filtering method. *IEEE Trans Power Delivery*. 2019;34(3):941-949.
28. Zhang H, Ruan X, Lin Z, Wu L, Ding Y, Guo Y. Capacitor voltage full feedback scheme for LCL-type grid-connected inverter to suppress current distortion due to grid voltage harmonics. *IEEE Trans Power Electron*. 2021;36(3):2996-3006.
29. Liu B, Wei Q, Zou C, Duan S. Stability analysis of LCL-type grid-connected inverter under single-loop inverter-side current control with capacitor voltage feedforward. *IEEE Trans Industr Inform*. 2018;14(2):691-702.
30. Yang D, Ruan X, Wu H. A real-time computation method with dual sampling mode to improve the current control performance of the $ LCL $-type grid-connected inverter. *IEEE Trans Ind Electron*. 2015;62(7):4563-4572.
31. Yang D, Ruan X, Wu H. Impedance shaping of the grid-connected inverter with LCL filter to improve its adaptability to the weak grid condition. *IEEE Trans Power Electron*. 2014;29(11):5795-5805.
32. Lai CM, Lin YJ, Cheng YH, Yao L. Development of a modular single-phase grid-tie inverter system for fuel-cell power generation. *J Chinese Instit Eng*. 2018;41(2):112-123.
33. Guoqiao Shen S, Xuancai Zhu Z, Jun Zhang Z, Dehong Xu. A new feedback method for PR current control of LCL-filter-based grid-connected inverter. *IEEE Trans Ind Electron*. 2010;57(6):2033-2041.
34. Padmanaban S, Priyadarshi N, Bhaskar MS, Holm-Nielsen JB, Hossain E, Azam F. A hybrid photovoltaic-fuel cell for grid integration with jaya-based maximum power point tracking: experimental performance evaluation. *IEEE Access*. 2019;7:82978-82990.
35. Mohiuddin SM, Macana CA, Pota HR, Hossen T, Mahmud MA. Nonlinear partial feedback linearizing controller design for grid-connected fuel-cell system with third harmonic injected PWM approach. *2017 North American Power Symposium (NAPS)*. IEEE. 2017:1-6.
36. Li Q, Chen W, Liu Z, Zhou G, Ma L. Active control strategy based on vector-proportion integration controller for proton exchange membrane fuel cell grid-connected system. *IET Renew Power Gen*. 2015;9(8):991-999.
37. Patra S, Narayana M, Mohanty SR, Kishor N. Power quality improvement in grid-connected photovoltaic–fuel cell based hybrid system using robust maximum power point tracking controller. *Electric Power Comp Syst*. 2015;43(20):2235-2250.
38. Yang Y, Guo X, Lu Z, Hua C, Castilla M, Blaabjerg F. Advanced control of grid-connected inverters for proton exchange membrane fuel cell system. *Int J Hydrogen Energy*. 2020;45(58):33198-33207.

How to cite this article: Hosseinpour M, Sabetfar T, Shahparasti M. Grid-tied PEMFC power conditioning system based on capacitor voltage thorough feedback procedure in a weak and harmonics-polluted network. *Energy Sci Eng*. 2024;12:149-167. doi:10.1002/ese3.1624

20500505, 2024, 1, Downloaded from https://scijournals.onlinelibrary.wiley.com/doi/10.1002/ese3.1624 by University Of Yazd, Wiley Online Library on [04/03/2025]. See the Terms and Conditions (https://onlinelibrary.wiley.com/terms-and-conditions) on Wiley Online Library for rules of use; OA articles are governed by the applicable Creative Commons License